Multidimensional Modeling of Turbulent Two-Phase Flows in Stirred Vessels

A. D. Gosman, C. Lekakou and S. Politis
Dept. of Mechanical Engineering, Imperial College, United Kingdom

R. I. Issa
Dept. of Mineral Resources Engineering, Imperial College, United Kingdom

M. K. Looney
Imperial Chemical Industries PLC, United Kingdom

This article outlines a computational procedure for the prediction of dispersed two-phase, solid-liquid and gas-liquid, turbulent flows in baffled, impeller-stirred vessels common in the chemical industries. A two-flow Eulerian model is employed, based on the main assumption of interpenetrating coexisting continua. Mean momentum and mass conservation equations are solved for each phase and turbulent closure is effected by extending the single phase k-ϵ turbulence model to two-phase flows. The resulting set of highly coupled equations is solved by a two-phase implicit algorithm, PISO-2P, which allows calculation for a wide range of phase fraction, particle size and phase density ratios. Predictions are presented for solid-liquid and gas-liquid (bubbly) flows. Comparisons are made with experimental data for the mean phase velocities and volume fraction, mean slip velocity and turbulence quantities.

Introduction

Background

Multiphase stirred tank reactors are widely encountered in the chemical process and allied industries. They consist of a cylindrical vessel, fitted with one or more motor-driven rotating impellers whose shape, positioning within the tank and speed of rotation varies widely according to the particular application. In most cases the vessel is fitted along its inner periphery with baffles whose purpose is to inhibit 'dishing' of the free surface, assist the mixing action and promote heat and/or mass transfer and/or chemical reaction as the case may be. A typical mixing vessel is shown diagrammatically in Figure 1.

Despite the widespread use of such equipment, the complexity of the flow generated within (3-D, recirculating and often turbulent) has compelled designers to resort to empirical information that has been amassed over the years (Nagata, 1975; Oldshue, 1983; Holland et al., 1966; Uhl et al., 1966) and often complement that with pilot plant experiments, in order to tackle the problems associated with the optimization and scale-up of existing processes and the design of novel ones. There are three important drawbacks in such practices: First, the available information is usually encoded in an overall/global parametric form effectively concealing detailed localized information; the latter may be crucial in the successful design of process equipment. Secondly, even for 'standard' processes, scale-up criteria are either incomplete or contradictory and may lead to unnecessarily expensive or even wrong solutions. Thirdly, if the design of a novel process is of interest, then extrapolation beyond the areas covered by the 'design charts' becomes inevitable; this is an inherently uncertain and often harzardous method.

From the above considerations, it is obvious that the development is desirable of a computational technique that predicts in considerable detail and accuracy the flowfield within mixing vessels under different operating conditions. Several such techniques have already been devised for the case of single phase flow; examples of such work can be found (Issa et al., 1981; Harvey et al., 1982; Placek et al., 1986; Kresta et al., 1991). Early developments in this area resorted to idealizations

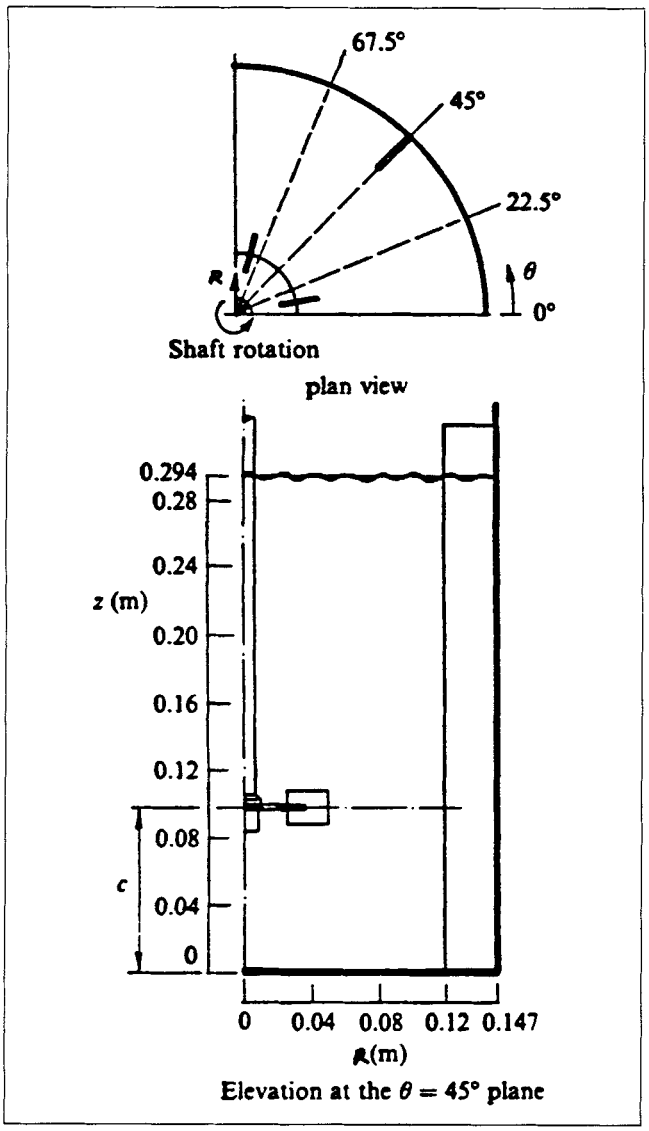

Figure 1. Mixing vessel configuration.

(some sweeping) in order to make the problem tractable. Here, one of the main difficulties lies in the representation of the impeller action which often had to be made by recourse to empiricism or to crude models. More recent developments (Kresta et al., 1991) have produced more sophisticated models for this action which obviously improve the quality of the prediction of the flow within the rest of the vessel. Considering their importance, predictive methods for turbulent two-phase flow in mixing vessels are much more scarce as noted below. This perhaps is not very surprising given the additional difficulties, both modeling and numerical, introduced by the presence of the second phase in an already complex flow. It is this kind of flow that this article addresses.

Previous work

Investigations involving two-phase flows in geometries other than stirred vessels are many and varied. Briefly, two main approaches can be distinguished in the analysis of the discrete phase. In the Lagrangian approach the trajectories of individual particles are predicted based on varying initial conditions, whereas in the Eulerian approach the particulate phase is treated as a continuum subject to appropriate boundary conditions. Applications where the discrete phase is present in significant proportions and is widely dispersed, favor the Eulerian approach from a numerical as well as physical point of view (for example, in the simulation of turbulent mixing processes in stirred vessels). While most studies stress the importance of proper modeling of the turbulence exchange mechanisms between the two phases, few workers (excluding studies where ad hoc adjustments to single-phase turbulence models were made) have addressed themselves to the closure of the Eulerian two-phase transport equations. Exceptions, however, are studies such as Pourahmadi et al. (1983), Mostafa et al. (1985), and Rizk et al. (1989) where two-phase turbulence closures were derived and applied to duct and jet flows at low solid volumetric loadings.

Three dimensional calculations with application to mixing vessels of the type used in this study have been previously performed by some of us for gas-liquid (Issa et al., 1981) and solid-liquid flows (Looney et al., 1985). In the former study, a simplified form of the gas phase momentum equation was employed and no turbulence modification due to the dispersed phase was considered. In the second study, a full two-phase turbulence closure was presented with the full equations solved for both phases. Preliminary comparisons against experimental data, albeit for coarse computational grids, were promising and demonstrated the viability of the methodology and the potential to extend it to calculations of gas-liquid systems. In what follows we describe the status of the modeling after further development and present the results of more extensive validation studies.

Mathematical Model

Instantaneous equations

We have considered two-phase systems consisting of a continuous liquid phase containing monodispersed solid particles or bubbles (in principle the analysis is readily extendible to more phases and/or polydispersed systems). A "two-fluid" model approach is adopted (Ishii, 1975) where both phases are assumed to coexist at every point in space in the form of interpenetrating continua. Transport equations for mass and momentum are formulated for each phase in volume averaged form. In orthogonal tensor notation they read:

$$(\rho^c\alpha^c)_{,t} + (\rho^c\alpha^c u_i^c)_{,i} = 0 \tag{1}$$

$$(\rho^d\alpha^d)_{,t} + (\rho^d\alpha^d u_i^d)_{,i} = 0 \tag{2}$$

$$(\rho^c\alpha^c u_i^c)_{,t} + (\rho^c\alpha^c u_i^c u_j^c)_{,j} = -\alpha^c P_{,i} + (\alpha^c \tau_{ij}^c)_{,j} + F_i^{cd} \tag{3}$$

$$(\rho^d\alpha^d u_i^d)_{,t} + (\rho^d\alpha^d u_i^d u_j^d)_{,j} = -\alpha^d P_{,i} + (\alpha^d \tau_{ij}^d)_{,j} - F_i^{cd} + \alpha^d(\rho^d - \rho^c)g_i \tag{4}$$

$$\alpha^c + \alpha^d = 1 \tag{5}$$

where

$$\tau_{ij}^c \equiv \mu^c \left\{ u_{j,i}^c + u_{i,j}^c - \frac{2}{3}\delta_{ij}\, u_{m,m}^c \right\} \tag{6}$$

$$\tau_{ij}^d \equiv \mu^d \left\{ u_{j,i}^d + u_{i,j}^d - \frac{2}{3}\delta_{ij}\, u_{m,m}^d \right\} \tag{7}$$

and the dispersed phase viscosity is obtained from empirical correlations appearing in Zenz et al. (1960), and Murray (1965) for the solid and in Ishii et al. (1979) and Zaber (1964) for the gas phase respectively. In turbulent flows such as those considered in this study the viscous stress terms are usually negligible.

The momentum exchange term, F^{cd}, consists of a linear combination of the mechanisms of momentum exchange between the phases, namely: drag, added mass, lift, Basset force and so on, each of which has to be modeled.

The drag force is modeled as:

$$F_i^D = \frac{3}{8R_p}\rho^c \alpha^d c_D V (u_i^d - u_i^c) \tag{8}$$

where $V = \sqrt{(u_i^d - u_i^c)^2}$ and the drag coefficient, c_D, is obtained from empirical correlations in terms of the particle Reynolds number appearing in Clift et al. (1971), Richardson et al. (1954), Ishii et al. (1979) and Zuber (1964). Following the formulation used in Winjgaarden (1976), the added mass effect is modeled as:

$$F_i^A = \{ c_A \alpha^d u_j^d (u_i^d - u_i^c) \}_j \tag{9}$$

where $c_A = \lambda \rho^c$ with $\lambda = 0.5\,(1 + 2.78\,\alpha^d)$ to account for multiple particle effects.

Models for the other forces were also examined but these effects were found to be of much less significance. This was established by an order of magnitude analysis which was carried out for each of the above contributions for conditions usually encountered in stirred vessels. Such an analysis is easily carried out but is not included here for brevity. The results of the analysis do show that for solid-liquid suspensions only the drag force component of F^{cd} is important. The same analysis shows that for gas-liquid flows both the drag and added mass forces are important relative to the rest. Furthermore, a posteriori calculation of the relative magnitudes of the various terms from the computations presented herein indeed verified the findings of the above mentioned analysis.

Turbulence modeling

Turbulent effects are modeled by time averaging Eqs. 1-5 in a way resembling the analysis of variable density single-phase flows (Jones, 1980). In particular, apparent density weighted averaging akin to 'Favre' averaging in compressible flows is employed. This practice has the merit of reducing the number of correlations emerging after the averaging operation as compared with conventional time averaging. The phase velocities are thus decomposed into phase mean and fluctuating components as $u = \tilde{u} + u''$ and all scalars are decomposed as $q = \bar{q} + q'$ with the definitions $\tilde{u} = \overline{\alpha u}/\bar{\alpha}$, $\overline{u''} \neq 0$, $\overline{q'} = 0 = \overline{\alpha u''}$, applying. All variables in Eqs. 1-5 are treated in a similar manner and the resulting equations are then time averaged.

In the averaged phase continuity equations no additional terms requiring modeling arise. In the continuous phase momentum equations four terms arise for which modeling is required. The Reynolds stresses are modeled using a suitably extended version of the well known k-ϵ turbulence model (Launder et al., 1972) as:

$$\overline{-\rho^c \alpha^c u_i^{c\,\prime\prime} u_j^{c\,\prime\prime}} = \mu_t \left[\tilde{u}_{i,j}^c + \tilde{u}_{j,i}^c - \frac{2}{3}\delta_{ij}\tilde{u}_{m,m}^c \right] - \frac{2}{3}\delta_{ij}\rho^c \bar{\alpha}^c k \tag{10}$$

where $\mu_t = \bar{\alpha}^c c_\mu \rho^c k^2/\epsilon$ with c_μ taking the value 0.09 from single-phase flow practice. The turbulence kinetic energy, k, and its rate of viscous dissipation, ϵ, appearing in the above are defined as:

$$k = \frac{\overline{\alpha^c u_i^{c\,\prime\prime} u_i^{c\,\prime\prime}}}{2\bar{\alpha}^c} \text{ and } \epsilon = \frac{\mu^c}{\rho^c}\frac{\overline{\alpha^c u_{i,j}^{c\,\prime\prime} u_{i,j}^{c\,\prime\prime}}}{\bar{\alpha}^c} \tag{11}$$

The correlation between the fluctuating phase fraction and pressure gradient, $\overline{-\alpha^{c\prime} P_{,i}'}$, is modeled according to single-phase variable density practices (Jones, 1980).

In the modeling of the remaining terms of the momentum equations the discrete phase fluctuating velocity is expressed in terms of its continuous phase counterpart via the following formula, derived from a Lagrangian analysis of a particle's response to eddies which are much longer than its diameter (Politis, 1989):

$$u^{d\prime} = u^{c\prime}\left(1 - \exp\left(\frac{-t_1}{t_p}\right)\right) \tag{12}$$

where t_1 is a measure of the mean eddy lifetime [typically $\approx 0.41k/\epsilon$ (Calabrese et al., 1979)] and t_p is the particle response time given by $[3/8R_p\,(\rho^c\,\alpha^d c_D V)]^{-1}$, with c_D given by the appropriate expression. This formula is obtained by the Lagrangian integration of the equation of motion of a particle moving through a fluid eddy of given velocity distribution. For particles that are of size comparable to or bigger than the eddy size, Eq. 12 may not, however, be valid. The above practice allows the discrete phase turbulent momentum fluxes, that is, $\overline{-\rho^d \alpha^d u_i^{d\,\prime\prime} u_j^{d\,\prime\prime}}$ to be expressed in terms of their continuous phase counterparts whose modeling is given by Eq. 10. Likewise all correlations involving the fluctuating velocities of both phases are reduced to expressions involving only those of the continuous phase. This is an important difference compared to alternative approaches (Pourahmadi, 1983; Elghobashi et al., 1983; Mostafa et al., 1985; Rizk et al., 1989), which model the discrete phase turbulent momentum fluxes by invoking Boussinesq type approximations but then encounter difficulties with the specification of the discrete phase momentum diffusivity.

The final main modeling assumption made is that of the gradient diffusion whereby all scalar turbulent fluxes are modeled as:

$$\overline{q' u_i'} = -\frac{\mu_t}{\sigma_q}\overline{q}_{,i} \tag{13}$$

The resulting modeled form of the phase mass and momentum conservation equations reads:

$$(\rho^c\overline{\alpha^c}\ \tilde{u}_i^c)_{,i}=0 \tag{14}$$

$$(\rho^d\overline{\alpha^d}\ \tilde{u}_i^d)_{,i}=0 \tag{15}$$

$$(\rho^c\overline{\alpha^c}\ \tilde{u}_i^c\tilde{u}_j^c)_{,j}=-\overline{\alpha^c}\overline{P}_{,i}+\{(\overline{\alpha^c}\mu^c+\mu_t)\Delta\tilde{u}_{ij}^c\}_{,j}-\frac{2}{3}\{\delta_{ij}\rho^c\overline{\alpha^c}k\}_{,j}$$
$$+A_D\left\{\rho^d\overline{\alpha^d}(\tilde{u}_i^d-\tilde{u}_i^c)-\frac{\rho^d\rho^c\mu_t}{\sigma_\alpha(\rho^c\overline{\alpha^c})^2}\overline{\alpha_{,i}^c}\right\}-P_1-P_2 \tag{16}$$

$$(\rho^d\overline{\alpha^d}\tilde{u}_i^d\tilde{u}_j^d)_{,j}=-\overline{\alpha^d}\overline{P}_{,i}+\{\overline{\alpha^d}\mu^d\Delta\tilde{u}_{ij}^d\}_{,j}$$
$$+\left\{\frac{c_t^2\rho^d\overline{\alpha^d}}{\rho^c\overline{\alpha^c}}\left(\mu_t\Delta\tilde{u}_{ij}^c-\frac{2}{3}\delta_{ij}\rho^c\overline{\alpha^c}k\right)+\right.$$
$$\left.(1-2\overline{\alpha^d})\frac{(\rho^c c_p)^2}{\rho^d\overline{\alpha^d}}\overline{\alpha_{,i}^c}\ \overline{\alpha_{,j}^c}\right\}_{,j}-A_D\left\{\rho^d\overline{\alpha^d}(\tilde{u}_i^d-\tilde{u}_i^c)-\frac{\rho^d\rho^c\mu_t}{\sigma_\alpha(\rho^c\overline{\alpha^c})^2}\overline{\alpha_{,i}^c}\right\}$$
$$+P_1+P_2+(\rho^d\overline{\alpha^d}-\rho^c\overline{\alpha^d})g_i \tag{17}$$

where $P_1=\overline{-\alpha^{c'}P'_{,i}}$ and P_2 is the added mass term given by

$$\{c_A\overline{\alpha^d}(\tilde{u}_i^c\ \tilde{u}_j^d-\tilde{u}_i^d\ \tilde{u}_j^d)\}_{,j}$$
$$-\left\{\frac{c_t\lambda(1-c_t)\overline{\alpha^d}}{\overline{\alpha^c}}(\mu_t\Delta\tilde{u}_{ij}^c-\frac{2}{3}\delta_{ij}\rho^c\overline{\alpha^c}k)\right\}_{,j}+$$
$$\left\{\left(\frac{c_p\rho^c}{\rho^d}\right)^2\frac{c_A}{\overline{\alpha^d}}\left(1-\frac{1}{c_t}\right)\overline{\alpha_{,i}^c}\ \overline{\alpha_{,j}^c}\right\}_{,j}$$

As noted above transport equations are derived for the turbulence quantities k and ϵ. They both contain a number of additional terms which originate from the interphase momentum exchange terms F^{cd} in the momentum equations and thus express modifications to the continuous phase turbulence due to the presence of the discrete phase. These terms are modeled in similar ways as in the phase momentum equations: space does not allow the details to be presented here. All other terms in the k, ϵ equations are modeled in ways analogous to single-phase practices with the constants retaining their single-phase values. The final equations read:

$$(\rho^c\overline{\alpha^c}\ k\tilde{u}_j^c)_{,j}=\left\{\left(\overline{\alpha^c}\ \mu^c+\frac{\mu_t}{\alpha_k}\right)k_{,j}\right\}_{,j}$$
$$+\left(\mu_t\Delta\tilde{u}_{i,j}^c-\frac{2}{3}\delta_{ij}\rho^c\overline{\alpha^c}\ k\right)\tilde{u}_{i,j}^c-\rho^c\overline{\alpha^c}\ \epsilon+\tilde{u}_i^cP_1+$$
$$A_D\left\{(c_t-1)2k\rho^d\overline{\alpha^d}+\left(2c_t-2-\frac{c_t}{\overline{\alpha^d}}\right)\overline{\alpha_{,i}^c}\ \overline{\alpha_{,i}^c}\right\}$$
$$+A_D(\tilde{u}_i^d-\tilde{u}_i^c)\frac{\rho^d\rho^c\mu_t}{\sigma_\alpha(\rho^c\overline{\alpha^c})^2}\overline{\alpha_{,i}^c} \tag{18}$$

$$(\rho^c\overline{\alpha^c}\epsilon\tilde{u}_j^c)_{,j}=\left\{\frac{\mu_t}{\sigma_\epsilon}\epsilon_{,j}\right\}_{,j}+(c_1G-c_2\rho^c\overline{\alpha^c}\epsilon)\frac{\epsilon}{k}$$
$$+2A_D(c_t-1)\epsilon\rho^d\overline{\alpha^d} \tag{19}$$

where G is the turbulence production equal to $\overline{-\rho^c\alpha^c u_i^{c''}u_j^{c''}}\ \tilde{u}_{i,j}^c$.

Boundary conditions

Impeller: Of prime importance in the computational model is the impeller treatment. A typical impeller is the Rushton turbine which creates a highly complex flow in its vicinity; the periodic unsteadiness of this flow and the existence of a pair of trailing vortices behind the impeller blades on either side of the impeller disk have all been confirmed experimentally (Van't Riet et al., 1973; Yianneskis et al., 1987) and an attempt to model the mean flow that fits the data of Van't Riet et al., (1973) has been reported (Placek, 1985). In previous studies (Issa et al., 1981; Harvey et al., 1982; Kresta et al., 1991) the impeller was represented as an inflow-outflow region across which profiles of the dependent variables were prescribed. The boundary condition treatment for the impeller region used in this study have been detailed elsewhere (Looney et al., 1985; Politis, 1989). Briefly, the circumferential velocity and levels of k and ϵ are imposed throughout the volume swept by the impeller blades by reference to the experimental data. All other variables are solved for within that volume as for any other part of the flow.

Solid Surfaces: No-slip boundary conditions are imposed on all solid surfaces for the continuous phase. They are introduced into the calculation via 'wall-functions' (Launder et al., 1974) based on a wall shear stress given by:

$$\tau_w=\frac{c_\mu^{0.25}\kappa\rho^c\overline{\alpha^c}\tilde{u}^c\sqrt{k}}{\ln(Ey^+)} \tag{20}$$

As a first approximation the same condition is also assumed to apply to the discrete phase and imposed in the corresponding momentum equations through an expression similar to Gosman (1969).

Free Surface: The free surface is assumed to be flat; it follows that the normal velocity, the tangential shear stresses, the normal fluxes of k and ϵ and the solid phase fraction gradient fall to zero at the surface. In gas-liquid systems however, the normal gas phase velocity is not zero. In such systems the most important axial forces acting on the gas phase near the free surface are the drag and the buoyancy forces. The bubbles are considered to reach the free surface at their terminal rising velocity and then to instantaneously burst unless conditions are such that bouncing will occur. In the latter case an empirical correction is applied.

Numerical methodology

The equations are solved by a finite volume method, whereby the solution domain is divided into control volumes or 'cells' formed from constant x, r and θ coordinate surfaces and discretization of the differential equations is effected by volume integration over each cell, using a staggered arrangement of variables (Gosman et al., 1969). The resulting equations connect the value of a variable ϕ at each cell-centered node to its nearest neighbors by algebraic relations of the form:

$$A_p\phi_p=\sum_n A_n\phi_n+S_p^\phi \tag{21}$$

where the subscripts 'p' and 'n' stand for the node in question and its neighboring nodes respectively, A's express the combined effect of convection and diffusion and S contains the source terms.

The phase momentum equations are coupled through the shared pressure field and the interphase momentum exchange terms, notably the drag and added mass force. This coupling is handled by means of the "PISO-2P" (**P**ressure **I**mplicit with **S**plitting of **O**perators **2**-**P**hase) implicit iterative algorithm which is an extension of the single phase precursor PISO algorithm (Issa, 1983) and has been successfully employed in other two-phase studies (Looney et al., 1985; Politis, 1985). A pressure equation is derived by combining the density-weighted overall continuity equation and the phase momentum equations. The resulting updated pressure field drives the phase velocities in the direction of satisfying continuity; this is achieved by a factorization technique which also handles the coupling between the phase momentum equations particularly through the drag. An updated phase fraction field is obtained by solving the discrete phase continuity equation. The iteration is completed by solving for the turbulence quantities k and ϵ for which the splitting procedure is also applied due to the strong coupling through their source terms.

The sets of discretized equations for each variable are solved iteratively by means of an ADI technique. The nonlinearities in the phase momentum and turbulence equations are catered for by standard under-relaxation techniques. The solution is considered converged when the residuals in the equations solved become smaller than a prescribed tolerance.

Application

Preamble

The computational model presented above has been successfully shown to be able to produce solutions for a range of operating conditions arising in stirred vessels for both solid-liquid and gas-liquid flows although only in a few instances, discussed below, was it possible to assess the accuracy, due to the limited availability of data. In the former case they include density ratios up to 5, particle sizes up to a fraction of a centimeter and volumetric holdups up to 40%. The impeller speed in all cases had to be high enough to keep the discrete phase well suspended as no mechanism for particle deposition and re-entrainment from the vessel bottom was built into the model. In the case of gas-liquid flows, bubble sizes of the order of a centimeter and holdups up to 20% were solved for. Also several computing meshes were tried, none of which as it turned out was fine enough to resolve all details of the flow field accurately.

In the next section results will be presented for a case of solid-liquid flow where experimental data were available (Nouri et al., 1992). The vessel geometric specifications are shown in Figure 1 and can be described compactly by the relation $C = D = T/3$ (cf. Table 1). Glass particles ($\rho^d = 2{,}950$ kg/m^3) of mean diameter 232.5 μm and a volumetric concentration of 0.02% were suspended in water. The impeller speed was 300 rpm corresponding to a Reynolds number ($\equiv \rho^c D^2 N/\mu^c$) of 48,000. The solution domain was covered by a 15,903 points computational mesh distributed as $31 \times 27 \times 19$ points in the axial, radial and circumferential direction respectively.

Table 1. Geometric Specifications (m) of the Mixing Vessels used in the Solid-Liquid and Gas-Liquid Studies

	H	T	L_b	D	C
s/l	0.294	0.294	0.0294	0.098	0.098
g/l	1.67	1.83	0.18	0.915	0.41

Results will also be presented for a gas-liquid case where experimental data for the void fraction distribution are available (Revill, 1987). The mixing vessel and the agitator were of the same shape as those in Figure 1 but of different dimensions given in Table 1. Air bubbles of 4 mm nominal diameter (corresponding to observations in experiment with which comparison is made) were injected from a 2.5 cm disc located on the vessel axis, 0.2 m from the base at a rate of 1,102 L/min in water; the impeller speed was 70 rpm. The bubbles were introduced into the computational domain as a source of gas momentum and mass at the appropriate location. The velocity of the gas bubbles was 18.8 m/s corresponding to experiment. However, it should be remarked that the gas injection velocity has little effect on the outcome as the gas stream enters directly into the impeller zone and its motion is then dictated by the strong impeller-imposed flow pattern. The assumption of a uniform bubble diameter is at variance with reality; breakup and coalescence ensure that bubble diameter is not constant. The justification for this assumption is that small changes in diameter around the nominal 4 mm should not influence slip velocity (and hence the drag force) much; this is inferred from the observed almost constant rise velocity of single bubbles in still liquid, for bubble diameters between 2 and 6 mm.

The computational mesh used in this case was formed by 8,100 points distributed as $27 \times 20 \times 15$ points in the axial, radial and circumferential direction respectively. The grid densities used in this study represent almost tenfold and thirtyfold increases, for solid-liquid and gas-liquid flows respectively, over previously reported computations (Looney et al., 1985; Issa et al., 1981). However, despite the improvement in flow resolution obtained from these grids, further grid refinement will be necessary in order to establish grid independent solutions.

Results and Discussion

Solid-liquid flows

The predicted mean velocity field is presented by means of liquid phase velocity vector plots obtained from projections of the 3-D velocity fields onto the vertical (x-r) and horizontal (r-θ) coordinate planes and shown in Figures 2, 3 and 4. The first plane is mid-way between baffles, and the second and the third are above and below the impeller respectively. Figure 2 exhibits the following features:

- A predominantly radial impeller stream with a slight upward tilt.
- Two ring vortices existing above and below the impeller stream; the lower vortex is stronger than the upper one due to the closer proximity of the impeller to the tank base.
- Mainly axial flow near the axis of the tank both above and below the impeller.

The three dimensionality of the flow is evident in Figures 3 and 4. Near the top of the vessel at $x = 0.908H$ there is a counter-rotating vortex in the wake of the baffle whereas the rest of

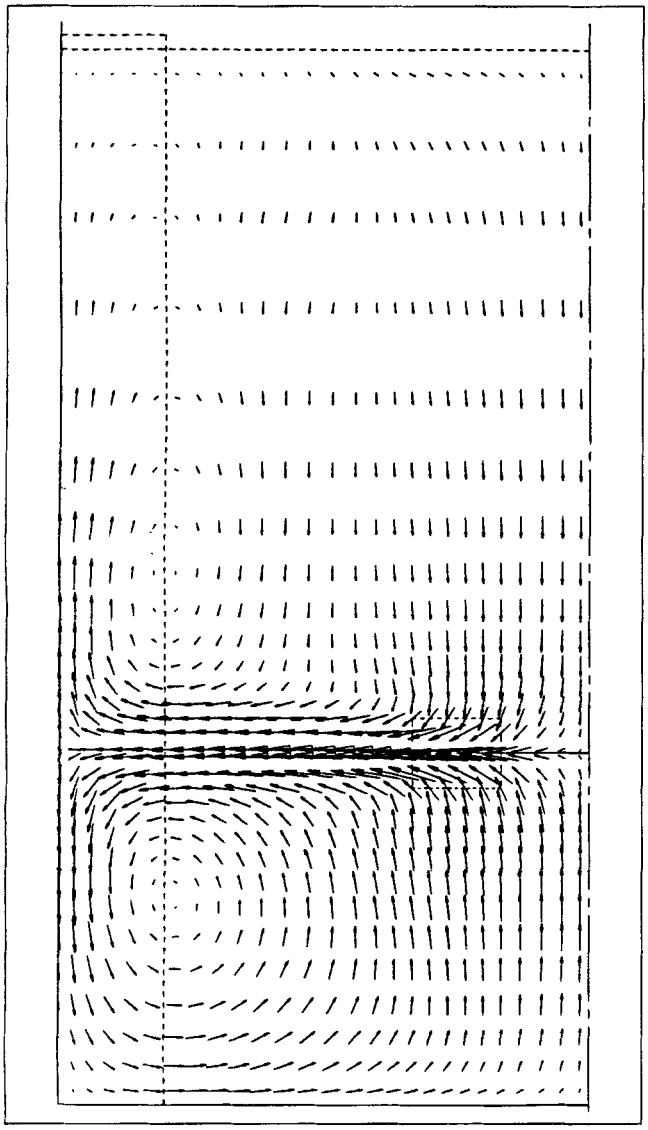

Figure 2. Velocity vectors @ θ = 0°; scale: → = 0.82 m/s.

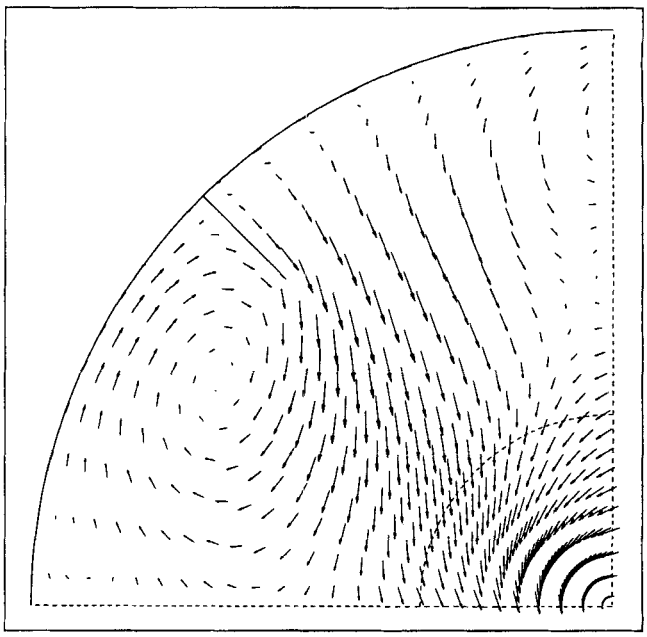

Figure 3. Velocity vectors @ x = 0.908H; scale: → = 0.15 m/s.

Comparisons of predicted mean velocities of the solid phase with the experimental data from Nouri (1992) are shown in Figures 7a, 7b and 7c. Both above and below the impeller the flow is well predicted. The comparison is less favorable in the downflowing wall jet whose strength is underpredicted by about 20%. This discrepancy is mainly attributed to the wall boundary condition imposed for the solid phase and the uncertainties associated with it. The mean radial velocity comparison in the immediate vicinity of the blade tip shows good agreement with the peak and spread of the impeller jet well captured. This

the flow is essentially radial and inwards directed. This contrasts sharply with the flow pattern immediately below the impeller at $x = 0.3H$ (Figure 4) where the flow is much stronger and is directed towards the vessel wall.

Figure 5 shows a plot of the slip velocity vector (u^S-u^l) in the x-r plane. The slip is uniformly aligned with the direction of gravity except in the immediate vicinity of the impeller and its magnitude is also uniform, at about 0.04 m/s which is very close to the terminal settling velocity of the particles. Further this plot indicates the regions of the vessel where the particles lead the fluid, for example in downflow, and *vice versa*.

Phase volume fraction contour plots of the solid normalized by the mean value are shown in Figure 6. As must be expected, the maximum solids fraction is predicted near the bottom of the tank, and the level progressively diminishes with increasing distance from the bottom to values in the upper region typically 1/6th of those in the lower region. This pattern is consistent with the magnitude and direction of the mean slip.

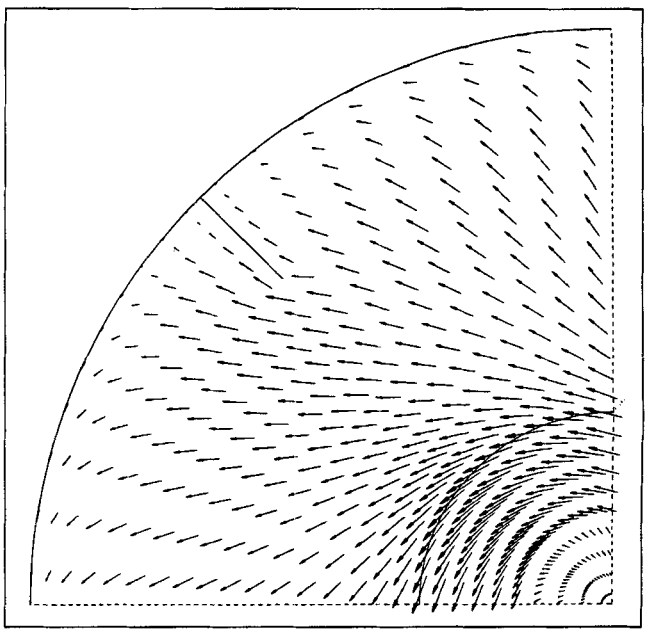

Figure 4. Velocity vectors @ x = 0.3H; scale: → = 0.63 m/s.

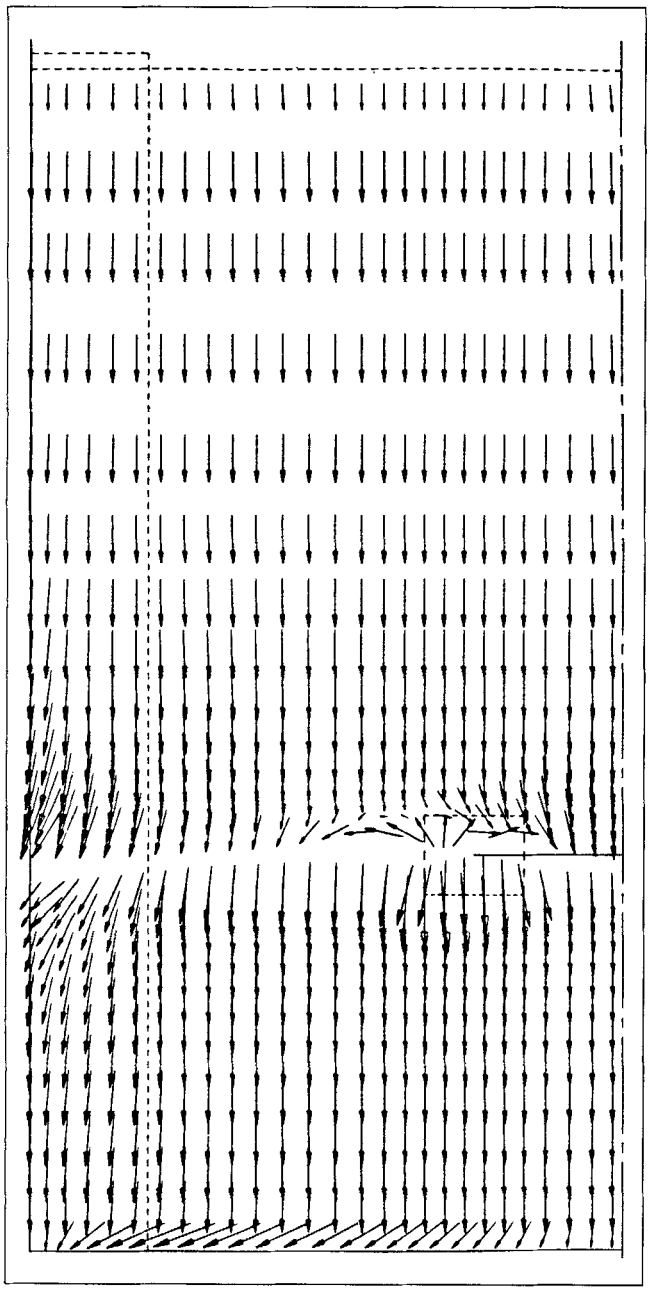

Figure 5. Slip velocity vectors @ $\Theta = 0°$; scale: → = 0.07 m/s.

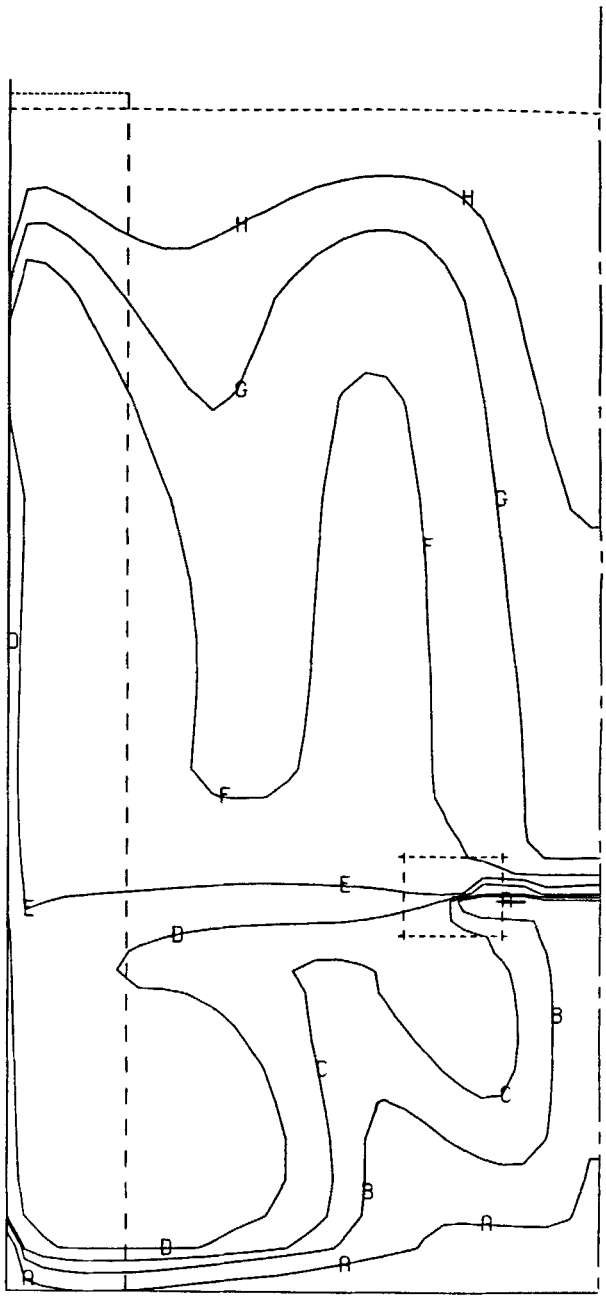

Figure 6. Normalized phase fraction contours @ $\Theta = 0°$; key: A = 6.0, B = 3.5, C = 2.5, D = 1.5, E = 1.0, F = 0.5, G = 0.3, H = 0.25.

serves as confirmation of the impeller boundary conditions applied to the solid phase. The rms velocity components comparisons are shown in Figures 8a, 8b and 8c respectively. Here qualitative agreement is obtained but quantitatively the predicted rms falls short of the measurements in the near wall region above the impeller and in the bulk of the vessel in the region below the impeller. It should be noted in this respect that the particle-eddy interaction model described earlier predicts that at best the local solid phase fluctuations are equal to their continuous phase counterparts. Hence the discrepancies noted above are attributed to similar discrepancies obtained in single-phase flow; they in turn are attributed to limitations in the k-ϵ model when applied to complex flows such as the one in a stirred vessel as well as limitations in the accuracy of the numerical scheme with regards to the differencing practice followed and the resolution accuracy of the mesh used (Politis, 1989). There is good agreement in the solid rms on exit from the impeller (Figure 8c), where in addition it is seen that the predicted solid rms lags that of the fluid because of the higher inertia of the particles.

Gas-liquid flows

The overall flow patterns (not shown) for this case are quite

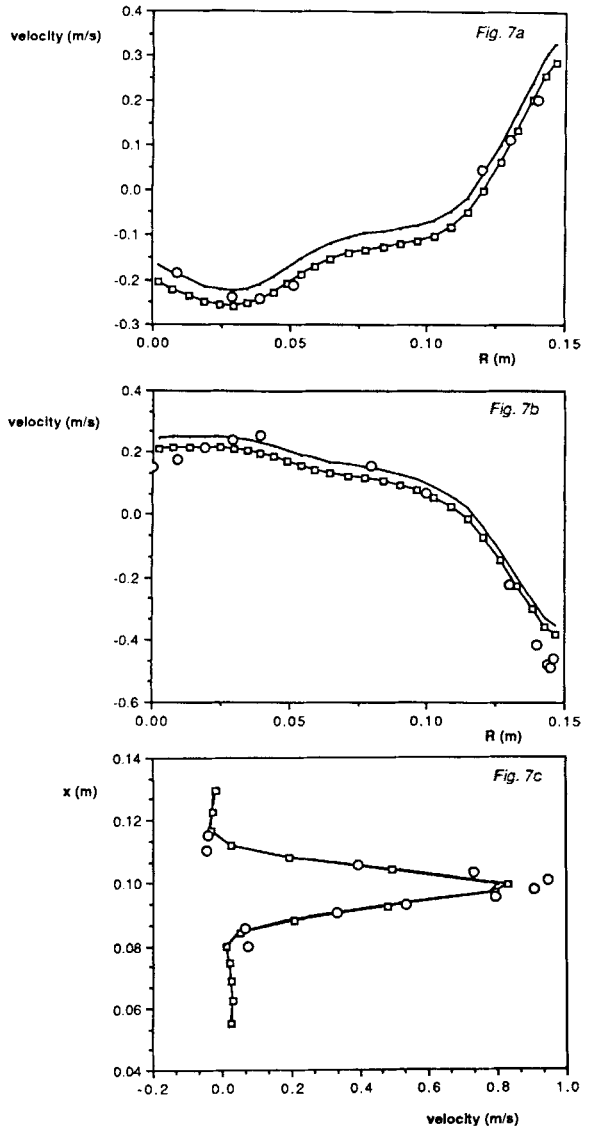

Figure 7. Mean velocity comparisons: (a) above the impeller @ x = 0.1203 m (axial); (b) below the impeller @ x = 0.0757 m (axial); (c) impeller stream @ R = 0.0515m (radial).

o Nouri (1992). -□- predicted solid phase, — predicted liquid phase.

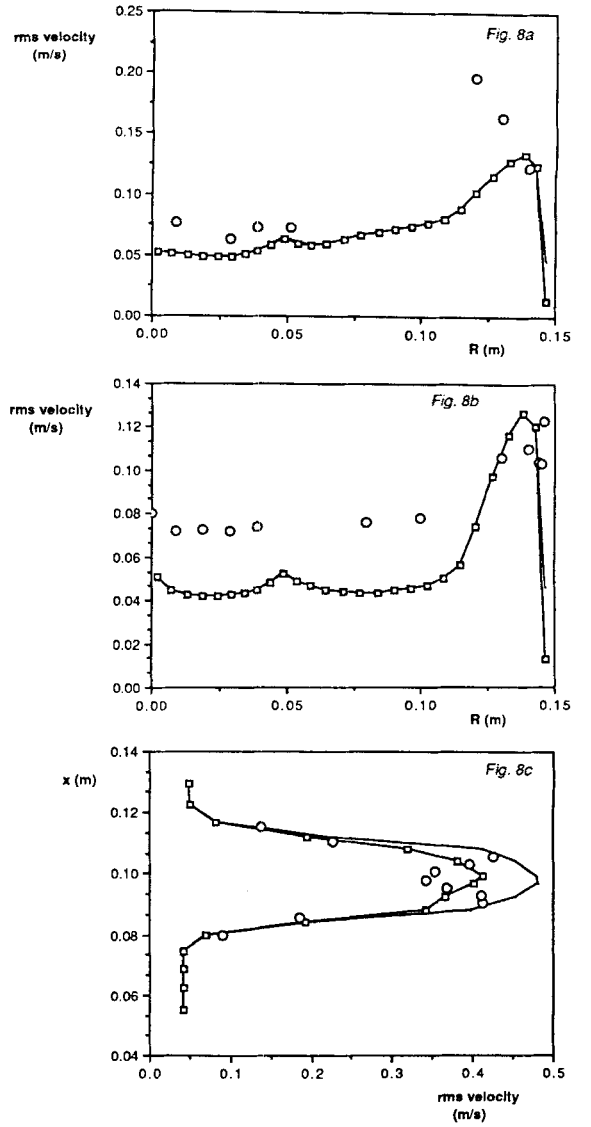

Figure 8. rms velocity comparisons: (a) above the impeller @ x = 0.1203 m (axial); (b) below the impeller @ x = 0.0757 m (axial); (c) impeller stream @ R = 0.0515 m (radial).

o Nouri (1992), -⊖- predicted solid phase, — predicted liquid phase.

similar to those displayed in Figures 2-4. Figure 9 shows predicted phase axial velocity profiles on the x-r plane at $\theta = 17.5°$ (that is, 27.5° upstream of the plane of the baffle, see also Figure 1). It is readily seen that the gas velocity profiles are always above those for the water due to the fact that the bubbles are lighter. Below the impeller and near the vessel axis, there is a sharp increase in the phase velocities due to the gas introduction there.

Figures 10a,b,c,d present comparisons of predicted void fraction profiles with experimental results on the x-r plane at $\theta = 15°$. Figure 10a shows profiles near the free surface and represents the influence of the free surface boundary conditions and the upper vortex dynamics. Figures 10b, c and d correspond to locations in the middle of the upper vortex, in the impeller stream and in the lower vortex respectively. Figure 10d shows relatively high void fractions predicted near the axis due to the gas introduction nearby; unfortunately there are no measurements in this region. The void fraction also increases near the wall because the flow there is enriched with bubbles entrained by the impeller jet. The void fractions in the lower vortex are generally lower than in the upper vortex due to the rising of the bubbles.

Figures 10c, 11a, 11b and 11c show comparisons between predicted and experimental void fraction profiles at $x = 0.41$ m and in the middle of the impeller stream, at different circumferential locations. There is a trend for the bubbles to accumulate at angular locations close to the baffle plane due to the flow field which is disturbed by the presence of the baffle. This trend is present in both the predicted and experimental results, but there is a substantial underprediction of

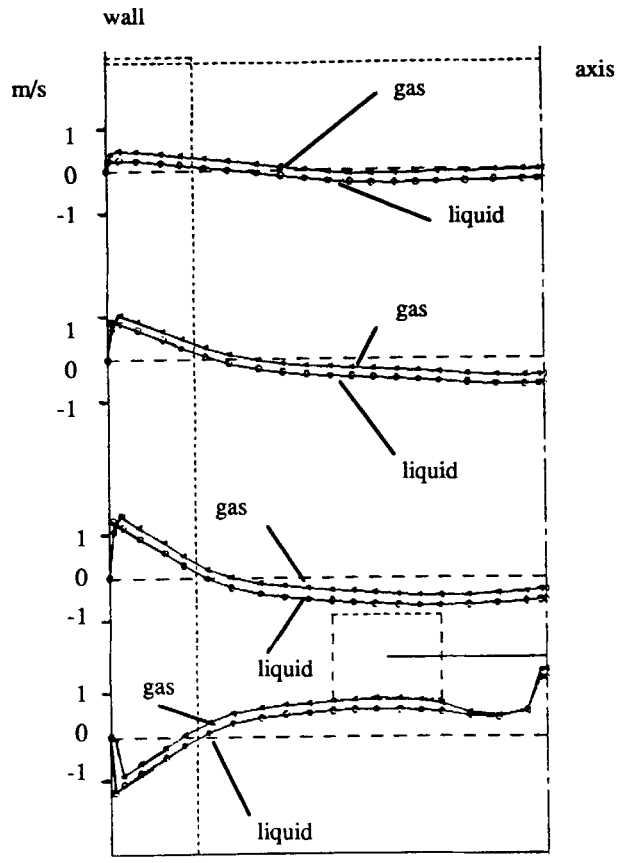

Figure 9. Radial profiles of axial velocity at different axial stations @ Θ = 17.5°.

the level at $\theta = 52°$ in connection with the reorganization of the flow in the baffle wake.

Apart from the possible inadequacy of the finest of meshes used to resolve the flow details completely, other factors related to modeling may be responsible for the discrepancy between predictions and experiment. In particular, the assumptions of a constant bubble diameter and a spherical bubble shape are suspect. These assumptions may have to be either relaxed or removed altogether if better representation of the physics is to be achieved. However, it is important that grid independence of the solution has to be established first before refinement of the models could be fruitfully pursued.

Overall the agreement with experiment is qualitatively good especially near the free surface. It can be seen that the predicted curves are generally lower than the experimental results. This may be due to the fact that the computational mesh used in these predictions for this vessel is relatively coarse compared to the solid-liquid case. A finer mesh is expected to result in better resolution of the profiles, according to experience of grid refinement in single-phase cases. There is also a possibility that the vessel contains bubbles smaller than the presumed 4 mm size: these would be less able to escape from the free surface and would thus tend to increase the void fraction level; this has been confirmed by test calculations.

Conclusions

A computational procedure for the prediction of turbulent

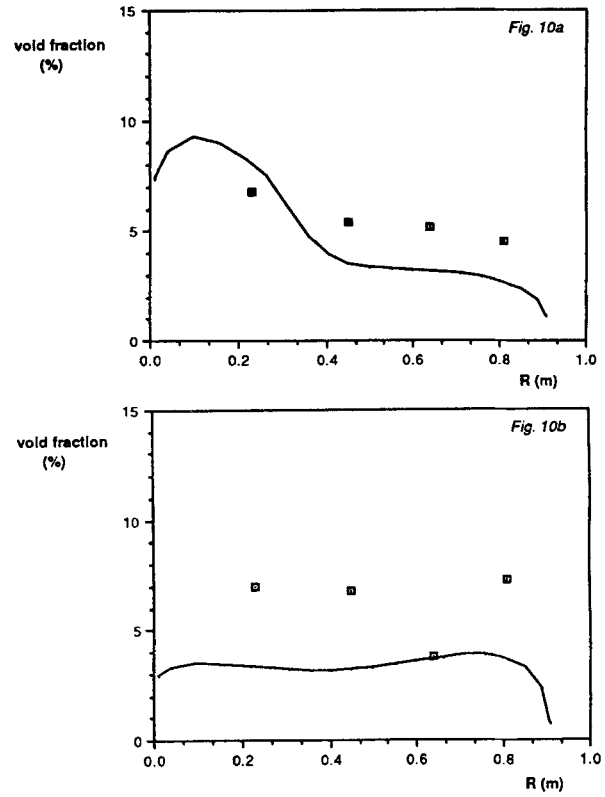

Figure 10a,b. Gas phase profiles @ Θ = 15°; (a) x = 1.52 m; (b) x = 1.04m.

⊡ Revill & Irvine (1987), — predictions.

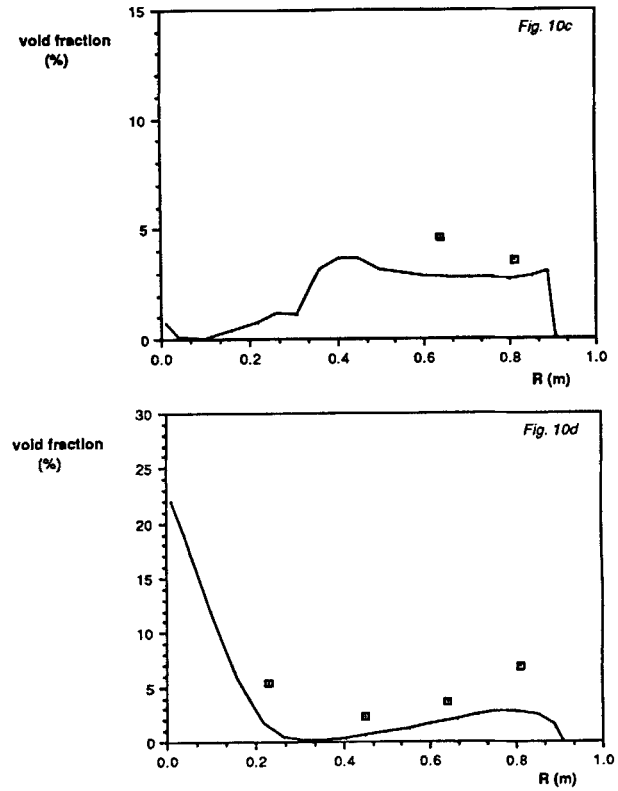

Figure 10c,d. Gas phase profiles @ Θ = 15°; (c) x = 0.41 m; (d) x = 0.12m.

⊡ Revill & Irvine (1987), — predictions.

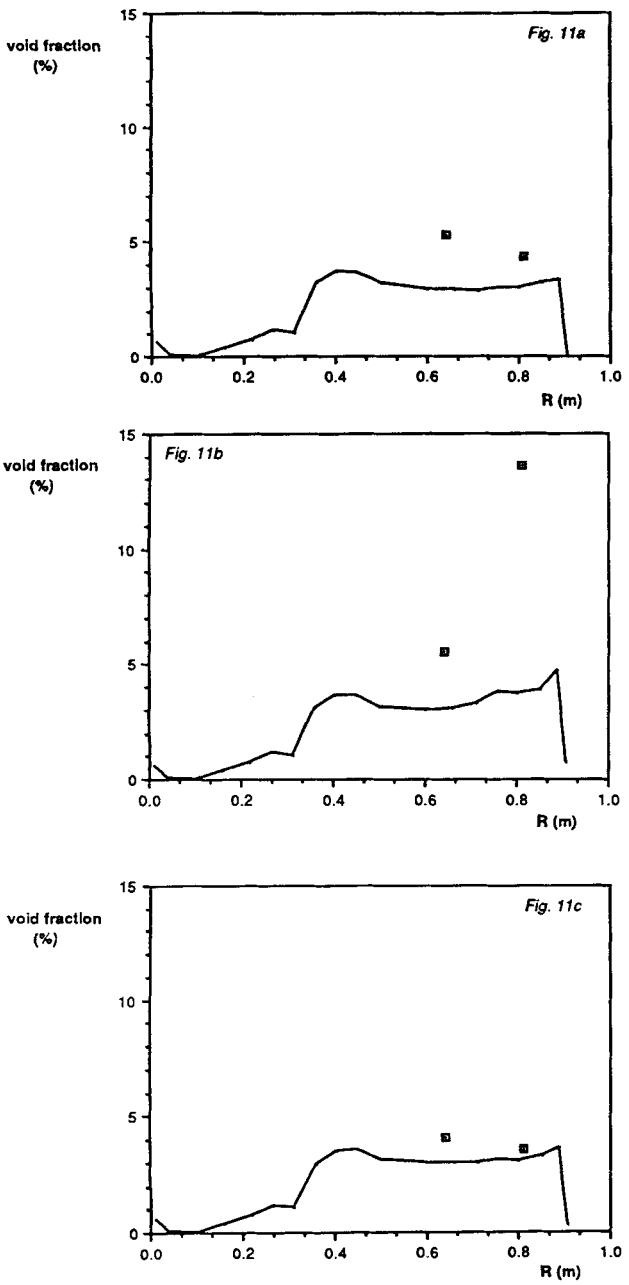

Figure 11. Gas phase profiles @ x = 0.41 m; (a) θ = 37.5°; (b) θ = 52.5°; (c) θ = 75°.

⊡ Revill & Irvine (1987), — predictions.

two-phase flows in stirred vessels has been described in some detail. Application to solid-liquid and gas-liquid flows demonstrates the capability of the method to produce physically realistic predictions of the flow and the phase distribution. Comparison of predictions against experimental data for such flows results in moderate quantitative agreement. However, further development and testing of the model for a variety of operating conditions is necessary before the method can be established as a reliable design tool. In this respect, the turbulence closure and therefore the prediction of the turbulence field throughout the vessel is important for the prediction of macro/micromixing phenomena, reaction yields, gas holdup, and impeller power consumption. Boundary conditions, primarily in the impeller region, play a major role in the above; improvements in their description in order to reduce the empirical input required, among other factors, will be beneficial to the method.

Acknowledgments

The authors would like to acknowledge the financial support provided by ICI plc, Unilever plc and the Commission of the European Communities.

Notation

A_p, A_n = central and neighboring node coefficients (c.f. Eq. 21)
A_D = $3\rho^c c_D V/(8\rho^d R_p)$
C = impeller disc clearance from the base of the mixing vessel
c_A = added mass force coefficient
c_D = drag force coefficient
c_μ = turbulence model constant equal to 0.09
c_p = $c_l\mu_l\rho^d/[\sigma_d(\rho^c\alpha^c)^2]$
c_t = $u^{d\prime}/u^{c\prime}$
c_1 = turbulence model constant equal to 1.43
c_2 = turbulence model constant equal to 1.92
D = impeller diameter
E = turbulence model constant equal to 9.0
F^A = added mass force
F^{cd} = phase interaction forces
F^D = drag force
g = gravity vector
H = height of mixing vessel
k = turbulence kinetic energy
L_b = baffle width
N = impeller speed
P = $p+\rho^c-\alpha^c g_i$
p = pressure
q = scalar quantity
R = radius of mixing vessel
R_p = particle radius
S^ϕ = source term appearing in Eq. 21
T = diameter of mixing vessel
t_l = eddy lifetime
t_p = particle response time
u = velocity vector
V = relative velocity
x, r, θ = cylindrical coordinates
y^+ = dimensionless distance from solid wall

Greek letters

α = phase fraction
Δu_{ij} = $u_{i,j}+u_{j,i}-2/3\delta_{ij}u_{k,k}$
δ_{ij} = Kronecker delta taking the value 1 when $i=j$ and 0 when $i\neq j$
ϵ = rate of viscous energy dissipation
κ = von Karman constant equal to 0.41
λ = added mass coefficient
μ = molecular viscosity
μ_t = turbulent viscosity
ρ = density
σ = turbulent Prandtl/Schmidt number: $\sigma_\alpha = 1$, $\sigma_\epsilon = 1.3$, $\sigma_k = 1$
τ_{ij} = stress tensor
τ_w = wall shear stress
ϕ = variable in Eq. 21

Superscripts

c = continuous phase
d = discrete phase
g = gas phase
l = liquid phase
s = solid phase

$\bar{}$, $'$ = denote mean and fluctuating quantities respectively, following Reynolds decomposition
$\sim$, $''$ = denote mean and fluctuating quantities respectively, following Favre decomposition

Subscripts

i, j, m = axes of coordinates
$,i$ = $\partial/\partial x_i$ and so on
n = neighbor node of a cell in the computational mesh
p = central node of a cell

Literature Cited

Calabrese, R. V., and S. Middleman, "The Dispersion of Discrete Particles in a Turbulent Flow Field," *AIChE J.*, **25**(6), 1025 (1979).

Clift, R., and W. H. Gauvin, "Motion of Entrained Particles in Gas Streams," *Canadian J. of Chem. Eng.*, **49**, 439 (1971).

Elghobashi, S. E., and T. W. Abou-Arab, "A Two-Equation Turbulence Model for Two-Phase Flows," *Physics of Fluids*, **26**(4), 931 (1983).

Gosman, A. D., W. M. Pun, A. K. Runchal, D. B. Spalding, and M. Wolfshtein, *Heat and Mass Transfer in Recirculating Flows*, Academic Press (1969).

Harvey, P. S., and M. Greaves, "Turbulent Flow in an Agitated Vessel," *Trans. Inst. Chem. Eng.*, **60**, 195 (1982).

Holland, F. A., and F. S. Chapman, *Liquid Mixing and Processing in Stirred Tanks*, Reinhold (1966).

Ishii, M., *Thermo-fluid Dynamic Theory of Two-phase Flow*, Eyrolles (1975).

Ishii, M., and N. Zuber, "Drag Coefficient and Relative Velocity in Bubbly, Droplet or Particulate Flows," *AIChE J.*, **25**(5), 843 (1979).

Issa, R. I., "Solution of the Implicitly Discretised Fluid Flow Equations by Operator Splitting," Imperial College Mechanical Engineering Dept. Report FS/82/15 (1983).

Issa, R. I., and A. D. Gosman, "The Computation of 3-D Turbulent Two-Phase Flows in Mixer Vessels," *Proc. 2nd Inter. Conf. on Numerical Methods in Laminar and Turbulent Flows*, Venice (1981).

Jones, W. P., "Models for Turbulent Flows with Variable Density and Combustion," in *Prediction Methods for Turbulent Flow*, W. Kollman, ed., Hemisphere Pub. Co. (1980).

Kresta, S. M., and P. E. Wood, "Prediction of the Three-Dimensional Turbulent Flow in Stirred Tanks," *AIChE J.*, **37**(3), 448 (1991).

Launder, B. E., and D. B. Spalding, *Mathematical Models of Turbulence*, Academic Press (1972).

Launder, B. E., and D. B. Spalding, "The Numerical Computation of Turbulent Flows," *Comp. Meth. Appl. Mech.*, **3**, 269 (1974).

Looney, M. K., A. D. Gosman, R. I. Issa, and S. Politis, "Modelling of the Turbulent Flow of Solid-Liquid Suspensions in Stirred Vessels," *5th Inter. Conf. of Mathematical Modelling*, Berkeley, CA (July 1985).

Mostafa, A. A., and S. E. Elghobashi, "A Two-Equation Turbulence Model for Jet Flows Laden with Vaporizing Droplets," *Int. J. of Multiphase Flow*, **11**(4), 515 (1985).

Murray, J. D., "On the Mathematics of Fluidization: Part 1. Fundamental Equations and Wave Propagation," *J. of Fluid Mechanics*, **21**(3), 465 (1965).

Nagata, S., *Mixing: Principles and Applications*, Halsted Press (1975).

Nouri, J. M., and J. H. Whitelaw, "Particle Velocity Characteristics of Dilute to Moderately Dense Suspension Flows in Stirred Reactors," *Int. J. Multiphase Flow*, **18**(1), 21 (1992).

Oldshue, J. Y., *Fluid Mixing Technology*, McGraw-Hill (1983).

Placek, J., and L. L. Tavlarides, "Turbulent Flow in Stirred Tanks, Part 1: Turbulent Flow in the Turbine Impeller Region," *AIChE J.*, **31**(7), 1113 (1985).

Placek, J., L. L. Tavlarides, G. W. Smith, and I. Fort, "Turbulent Flow in Stirred Tanks," *AIChE J.*, **32**(11), 1771 (1986).

Politis, S., "Prediction of Two-Phase Solid-Liquid Turbulent Flow in Stirred Vessels," PhD Thesis, University of London (1989).

Pourahmadi, F., and J. A. C. Humphrey, "Modelling Solid-Fluid Turbulent Flows with Application to Predicting Erosive Wear," *PCH*, **4**(3), 191 (1983).

Revill, B. K., and K. Irvine, "Measurement of Local Gas Phase Fraction in a Stirred Tank," ICI plc, private communication (1987).

Richardson, J. F., and W. N. Zaki, "Sedimentation and Fluidization, Part 1," *Trans. Inst. Chem. Engs.*, **32**, 35 (1954).

Rizk, M. A., and S. E. Elghobashi, "A Two-Equation Turbulence Model for Dispersed Dilute Confined Two-Phase Flows," *Int. J. of Multiphase Flow*, **15**(1), 119 (1989).

Uhl, V. W., and J. B. Gray, *Mixing: Theory and Practice*, Academic Press (1966).

Van't Riet, K., and J. M. Smith, "The Behaviour of Gas-Liquid Mixtures Near Rushton Turbine Blades," *Chem. Eng. Sci.*, **28**, 1031 (1973).

Winjgaarden, L., "Hydrodynamic Interaction between Gas Bubbles in Liquid," *J. of Fluid Mechanics*, **77**(1), 27 (1976).

Yianneskis, M., Z. Popiolek, and J. H. Whitelaw, "An Experimental Study of the Steady and Unsteady Flow Characteristics of Stirred Reactors," *J. of Fluid Mechanics*, **175**, 537 (1987).

Zenz, F. A., and D. F. Othmer, *Fluidization and Fluid Particle Systems*, Reinhold (1960).

Zuber, N., "On the Dispersed Two-Phase Flow in the Laminar Regime," *Chem. Eng. Sci.*, **19**, 897 (1964).

Manuscript received Aug. 28, 1991, and revision received July 27, 1992.